EUROPEAN LABORATORY FOR PARTICLE PHYSICS

CERN–PH–EP / 2004–021
May 7, 2004

Operation and Performance of the NA60 Silicon Pixel Telescope

K. Banicz[1,a)], A. David[1,2)], M. Floris[3)], J. M. Heuser[4)], M. Keil[1)], C. Lourenço[1)], H. Ohnishi[4)], E. Radermacher[1)], R. Shahoyan[2)], G. Usai[3)]

Abstract

The NA60 experiment studies open charm and prompt dimuon production in proton-nucleus and nucleus-nucleus collisions at the CERN SPS. The high multiplicity of charged tracks produced in heavy-ion collisions imposes the use of silicon pixel detectors to perform an efficient tracking. This paper describes the design and assembly of the pixel telescope and performance results from three detector planes operated in the high charged particle multiplicity conditions of Pb-Pb collisions.

Submitted to Nucl. Instr. and Meth. A

[1)] CERN, Geneva, Switzerland
[2)] CFIF - Instituto Superior Técnico, Lisbon, Portugal
[3)] Università di Cagliari and INFN, Cagliari, Italy
[4)] RIKEN - The Institute of Physical and Chemical Research, Wako, Saitama, Japan
[a)] Now at Universität Heidelberg, Heidelberg, Germany

1 Introduction

The NA60 experiment [1] aims at studying the production of prompt dimuons and open charm in proton-nucleus and heavy-ion collisions at the CERN SPS. New state-of-the-art silicon detectors in the vertex region complement the muon spectrometer and zero degree calorimeter previously used in NA50. A radiation tolerant beam tracker, based on silicon microstrip detectors operated at 130 K, measures the transverse coordinates of the incident ions with a precision of approximately 20 μm. Together with the information from the vertex pixel telescope this allows us to measure the offset of the muon tracks with respect to the event vertex and thereby distinguish events where a pair of D mesons was produced in the collision.

2 The NA60 Silicon Pixel Telescope

Downstream of the target and inside a 2.5 T magnetic dipole field, a silicon tracking telescope measures the charged tracks and allows us to identify which of them provide the best match with the muons measured in the muon spectrometer, which is placed behind a hadron absorber. For proton runs, this tracking telescope can consist of silicon microstrip planes, whereas the high particle multiplicity in heavy ion collisions imposes the use of silicon pixel detectors.

The pixel telescope of the NA60 experiment consists of 16 independent detector planes with 96 pixel chip assemblies in total, arranged along the beam axis over a length of $\sim$26 cm, starting at $\sim$7 cm downstream of the centre of the target. To optimally subtend the angular acceptance of the muon spectrometer, $3 < \eta < 4$ or $35 < \theta < 120$ mrad, the first planes are smaller than the last ones. Figure 1 shows the arrangement of the pixel detector planes. Each plane consists of several single-chip

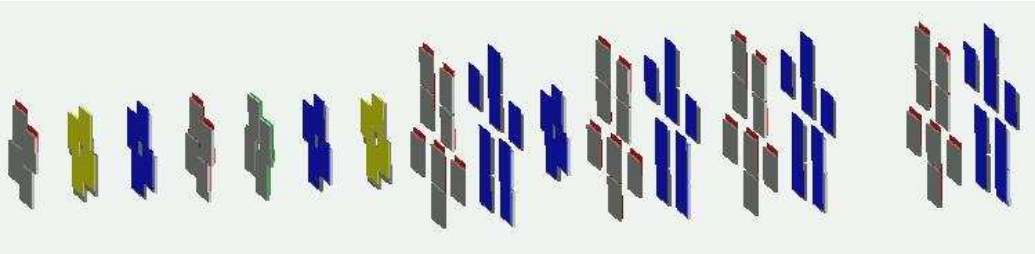

Figure 1: The complete vertex telescope, consisting of 4-chip and 8-chip planes. The beam comes from the left.

pixel detector assemblies which are mounted on a planar ceramic support ('hybrid'). The assemblies are made from radiation tolerant, 750 μm thick ALICE1LHCb pixel readout chips [2], bump bonded to 300 μm thick p-on-n silicon pixel sensors with 425×50 μm^2 pixels. The detector planes closest to the target comprise 4 of such assemblies, while the planes further downstream comprise 8 assemblies per ceramic,

with two ceramics mounted back-to-back to form one logical plane (Fig. 2). Since the pixel cells are not square, they measure one of the coordinates of the hit, x or y, with a better precision, depending on their orientation when positioned on the planes. To optimise the tracking and vertexing performance of the pixel telescope, the small planes exist in 'x' and 'y' versions, while the large ones are all 'x', having the best resolution coordinate perpendicular to the magnetic field lines, to optimise the momentum measurement. Some planes are placed with inverted orientation to maximise the overall angular acceptance coverage.

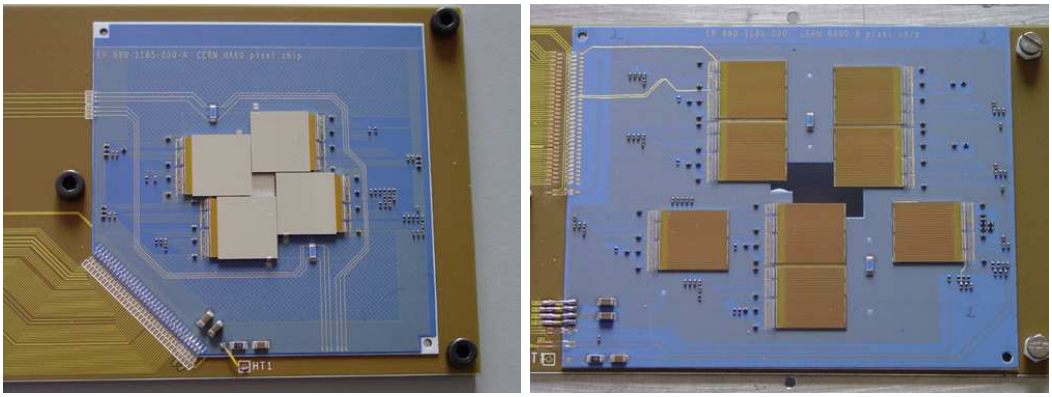

Figure 2: A 4-chip (left) and an 8-chip hybrid (right).

Each of the single chip assemblies consists of a matrix of 32 columns and 256 rows, resulting in a total of 8192 pixels. In the readout chip, every pixel cell contains a preamplifier, a shaper and a discriminator, as well as control and readout logic to transfer the binary hit information to the wire bond pads at the edge of the chip [2]. The collected and amplified charge is digitised by the discriminator whose threshold can be set by a global 8-bit voltage DAC and individually adjusted for each pixel cell by a local 3-bit DAC. Four "test" columns have additional diagnostic outputs at different stages of one readout cell. The chip is operated at 10 MHz and read out over 32 parallel data lines. The chips on one plane are read out sequentially. The chips were produced in a 0.25 μm technology and have been shown to remain fully functional after exposure to radiation doses of at least 12 Mrad [3]. Therefore, the detector should cope with the radiation levels of $\sim$ 1 Mrad per week expected in the cells closest to the beam axis on the first planes of the NA60 pixel telescope.

The readout chips are glued to the multilayer hybrid circuit fabricated on Al_2O_3 or BeO substrates. The ceramic support itself is glued and wire bonded onto a printed circuit board that provides mechanical support and routes all signals between the front-end electronics and the data acquisition, control and power supply systems. The circuit boards, mounted on aluminium frames, fit into slots of a support box between the dipole magnet shims, defining the detector positions with respect to the targets. The modules are cooled by water at $\sim$ 12 °C circulating in a copper tube attached to the back of the hybrid. Three 4-chip planes were used in the October

2002 Pb run. Figure 3 shows a fully mounted 4-chip plane with the aluminium frame and cooling tubes.

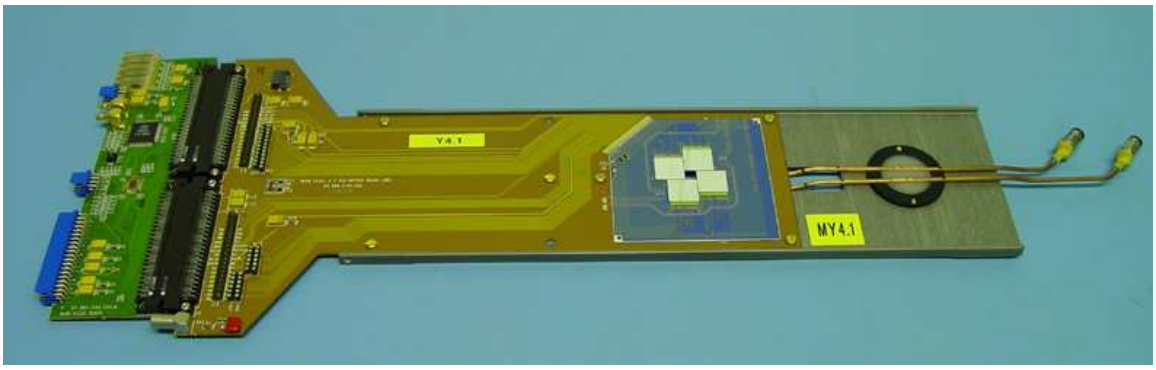

Figure 3: A 4-chip pixel detector plane with aluminium frame and cooling tubes.

3 Tests of Assemblies and Modules

Prior to the installation in the experiment, comprehensive quality assurance and system tests were performed in the laboratory. Electrical tests and measurements with radioactive sources yielded threshold behaviour, the number of dead pixels and pixels with missing bump connections of the individual assemblies. Assemblies with more than 96% of pixels working were used for the construction of the planes. The assembled planes were then tested and calibrated electrically for the operation in the experiment, using the internal pulser of the readout chip. Maps of dead and noisy pixels were prepared using a ^{90}Sr source.

A common threshold voltage for all pixels in the ALICE1LHCb chip is set by an internal DAC called pre_VTH. The actual threshold value for a given pre_VTH setting is measured by injection of test charges with a varying pulse height. Measuring the response of single pixels as a function of the pulse height gives integrated gaussian distributions whose 50%-point defines the pixel threshold, whereas its width corresponds to the electronics noise. Figure 4 shows how the measured average threshold depends on the value set on the pre_VTH DAC, for each pixel chip assembly of a given plane. One can see a linear behaviour of the measured average threshold with the pre-set value of the pre_VTH DAC. Thanks to low noise values and small pixel-to-pixel variations of the threshold, a nominal threshold value of 2000 e could be used in the experiment. The measured thresholds for a whole plane at this threshold setting can be seen in Fig. 5. The measurement shown yielded a threshold distribution with a mean value of 1930 e and a width of 260 e. No fine-tuning of individual pixel thresholds was applied at this stage.

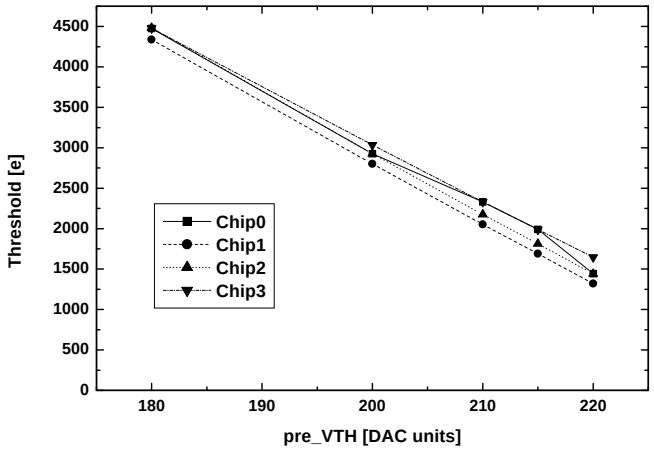

Figure 4: Threshold calibration for all chips of a pixel detector plane. The measured average thresholds show a linear dependence on the setting of the global threshold DAC. The value of this DAC can be adjusted individually for every chip.

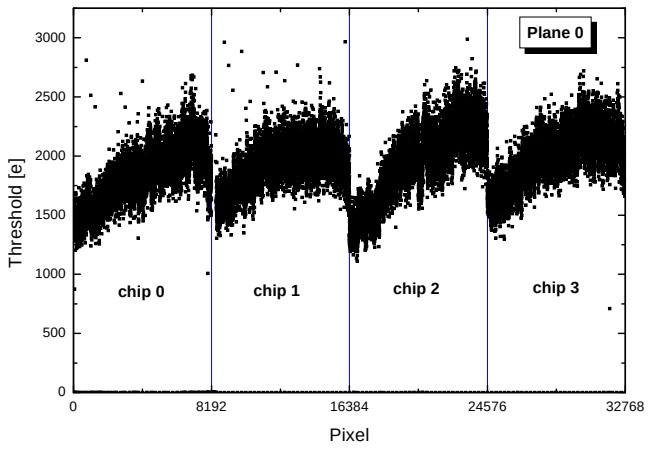

Figure 5: Measured thresholds for all pixels of a 4-chip plane, for a nominal threshold of 2000 e and without pixel-to-pixel threshold adjustment.

4 Results from the 2002 Lead Ion Run

Three 4-chip pixel detector planes were operated in the NA60 experiment in October 2002, with Pb-Pb collisions, 5 days at 30 and 5 days at 20 GeV per incident nucleon. The target system in this run consisted of three Pb targets of 0.5, 1.0 and 1.5 mm thickness. The pixel detector planes were positioned at 7.8, 10.1 and 13.1 cm downstream from the centre of the target box. The trigger, either "minimum bias" or "interaction", was provided by the zero degree calorimeter of NA60.

Figure 6 shows the number of reconstructed tracks for minimum bias Pb-Pb collisions. A relatively high track density of up to 100 or more tracks per event can be seen, leading to an occupancy of up to 2×10^{-2} hits per pixel per trigger in the pixels close to the beam hole of the detector planes. Figure 7 shows a typical hit map in one plane, integrated over several minutes.

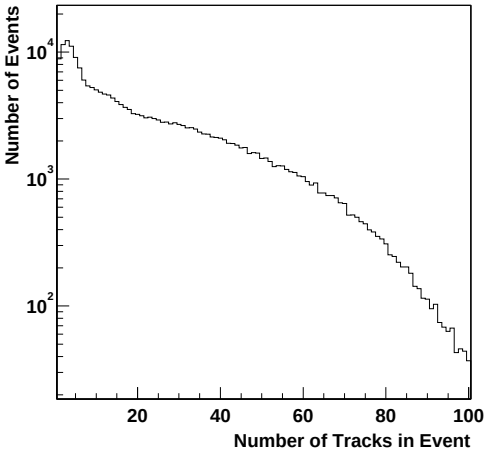

Figure 6: Distribution of the number of tracks per event reconstructed in the vertex telescope.

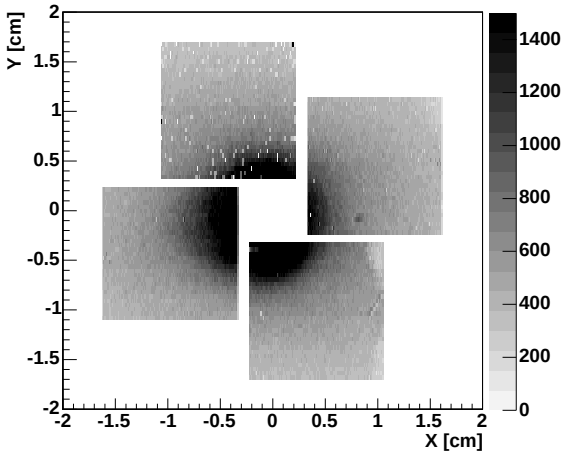

Figure 7: Hit map of a pixel detector plane integrated over several minutes of Pb-Pb running.

4.1 Cluster Sizes

The behaviour of the cluster sizes has been studied in detail for all three planes since it is directly related to the detector occupancy and could be a limiting factor in forthcoming heavy ion runs. Furthermore, a good understanding of the cluster size can be helpful in monitoring the effects of radiation damage in the silicon sensors during long data taking periods at high interaction rates.

The data shows that the cluster size mainly depends on three factors:

Track angle — Figure 8 shows the average cluster size versus the slope of the track with respect to the short pixel direction. To exclude the effect of bigger clusters

due to delta electrons, clusters of more than three pixels were excluded. The plot shows the behaviour expected from geometrical considerations: with increasing track inclination the number of neighbouring pixels crossed by the particle, and thus the cluster size, increases.

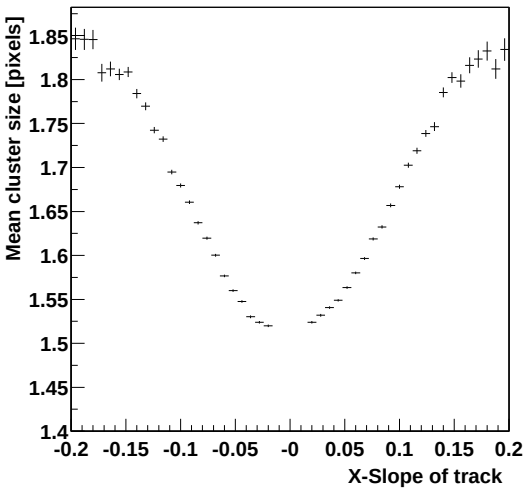

Figure 8: Dependence of the mean cluster size on the slope of the track with respect to the short pixel direction. For inclined tracks the charge tends to be deposited in several pixels.

Charge collection — As can be seen from Fig. 9, the average cluster size increases with increasing bias voltage, until the detector reaches the expected point of full depletion (between 30 and 40 V). A further increase of the bias voltage leads to a faster charge collection and to a smaller charge spread parallel to the sensor surface, resulting in a decrease of the cluster size.

Applied threshold — Figure 10 shows the dependence of the cluster size on the setting of the discriminator threshold. As expected, the cluster size decreases with increasing threshold since, especially in big clusters, many pixels collect only small fractions of the signal charge.

The behaviour of the cluster sizes can, to a good extent, be understood by the effects described above. The threshold setting can be used to lower the occupancy of the pixel planes when necessary, provided the efficiency does not change when increasing the threshold (discussed below).

4.2 Track Reconstruction

The spatial resolution and the efficiency of the pixel detector were assessed as follows. In a first step all tracks in the vertex telescope were reconstructed for a given event,

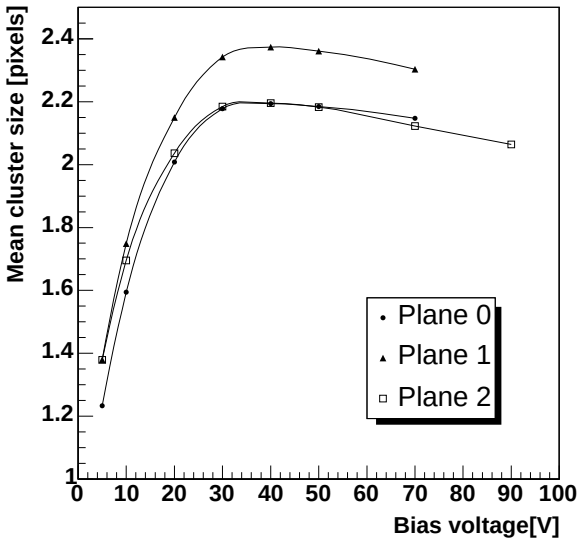

Figure 9: Dependence of the mean cluster size on the detector bias voltage, for the three planes.

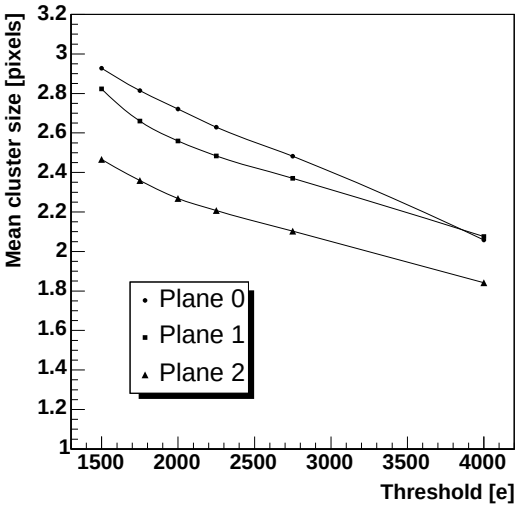

Figure 10: Dependence of the mean cluster size on the nominal discriminator threshold for all three planes.

requiring that each track has hits in all three planes. After identifying all vertices inside the target region, the vertex with the largest number of attached tracks was chosen. Then a second track reconstruction was done, this time requiring hits in all planes except the one whose efficiency and resolution was to be determined. Furthermore, an attachment to the vertex found in the first step was required, to reduce the combinatorial background. The tracks found in this step were extrapolated onto the plane under study, and that plane was checked for the presence of a hit in the

neighbourhood of the extrapolation point. If no cluster could be found within 3 σ of the track extrapolation, the chip was considered inefficient for this track.

4.2.1 Efficiency

Figure 11 shows the efficiencies determined for a single chip versus the y position, corresponding to the chip columns, of the extrapolated track. The efficiency is almost 100 % except for the regions of the so-called "test" columns, whose efficiency was compromised by non-optimised DAC settings.

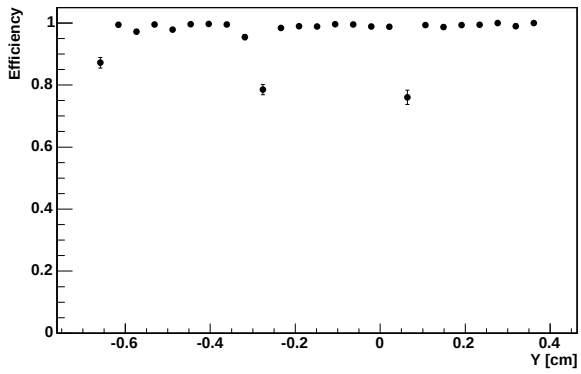

Figure 11: Efficiency measured for one chip of plane 1. The regions of lower efficiencies are due to the existence of "test" columns. Their efficiencies can be much higher when using fine tuned chip settings, not done when the data was taken.

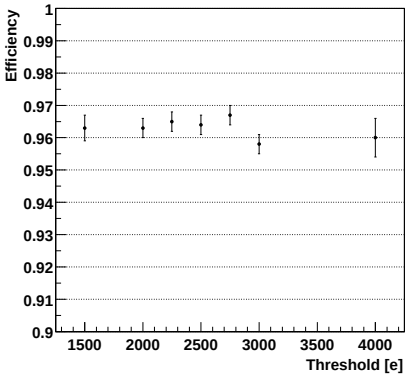

Figure 12: Dependence of the measured efficiency on the setting of the discriminator threshold. The efficiency has been averaged over the complete chip, including the test columns.

Figure 12 shows the average efficiency of a complete chip, including the test columns, measured during a threshold scan. We can see that, for thresholds between 1500 e and 4000 e, the efficiency stays constant within the precision of the measurement. This was expected since the average charge of more than 30 ke deposited in the sensor is much larger than the thresholds set.

4.2.2 Spatial Resolution

Comparing the positions of the extrapolated track points with the hits found in the plane under study yields residual distributions, from which we can derive the spatial resolution. An example of such a distribution is shown in Fig. 13 for the 50 μm pitch direction. The distribution can be described by a convolution of the intrinsic resolution of the pixel plane under study with the resolution function of the track extrapolation. The width of the residual distribution is approximately 13 μm for both 1-pixel and 2-pixel clusters. The similar widths of the distributions is in good

agreement with the equal fractions of 1 and 2-pixel clusters observed in the data. The contribution of the track resolution to the width of the residual distribution was estimated assuming that for a given cluster pattern the spatial resolution is equal in all three planes. Under this assumption we could deconvolute the two contributions, obtaining an intrinsic spatial resolution of approximately 10 μm for both 1 and 2-pixel clusters.

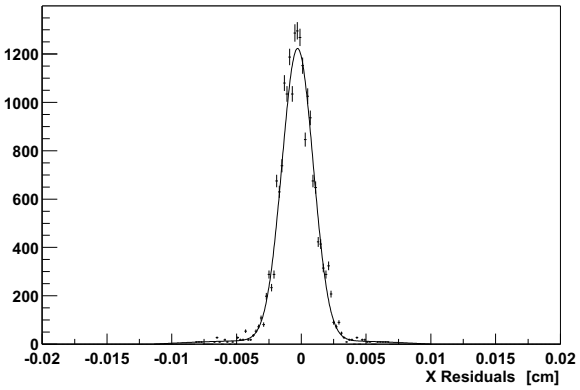

Figure 13: Residual distribution of 1-pixel clusters in one chip, for the 50 μm pitch direction.

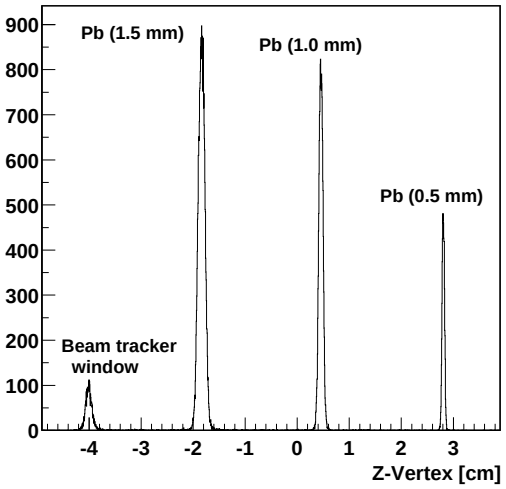

Figure 14: Z positions of the vertices as measured with the pixel telescope. The peaks correspond to the Pb targets and material from the beam tracker cryostat window.

4.3 Tracking performance

The tracks measured in the pixel telescope have been used to determine the position of the collision vertices. Figure 14 shows the distribution of the longitudinal coordinate

of the reconstructed vertices. The three Pb targets, as well as the cryostat exit window of the beam tracker, are clearly visible. The distributions for the three targets can be described by a convolution of the target density function and the gaussian resolution function of the vertex reconstruction. Deconvolution leads to the measured thickness of the targets and to the reconstruction resolutions listed in Table 1.

	Target 1	Target 2	Target 3
Z resolution	0.51±0.01 mm	0.32±0.01 mm	0.21±0.03 mm
Thickness	1.49±0.01 mm	0.98±0.01 mm	0.48±0.02 mm

Table 1: Z-vertex resolutions and thicknesses of the targets determined from the measured Z-vertex distribution.

Due to multiple scattering and increasing extrapolation distance, the reconstruction error increases from ~ 200 to ~ 500 μm when going to the most upstream target. The target thicknesses extracted from the deconvolution are in good agreement with the actual values of 1.5, 1.0 and 0.5 mm. The precision of the vertex reconstruction depends on the number of tracks associated with the vertex, as shown in Fig. 15 for the most downstream target. The plot shows the Z-vertex resolution versus the number of tracks. The data points were fitted with a function of the form

$$\sigma = \frac{\sigma_0}{\sqrt{N_{\text{Tracks}} - 1}} \tag{1}$$

resulting in the value $\sigma_0 = 1050 \pm 30$ μm.

Figure 16 shows the correlation between the x transverse coordinate of the vertex as measured in the pixel telescope and the same coordinate determined with the beam tracker. The correlation width is approximately 30 μm, including the tracking resolution of the beam tracker and the vertex resolution of the pixel telescope. Assuming a beam tracker resolution of 20 μm, one obtains a transverse vertex resolution of the pixel telescope of approximately 20 μm, for minimum bias collisions. Like the Z-vertex resolution, the transverse coordinate resolution improves for the most central collisions.

5 Summary

In October 2002, NA60 tested the first three planes of its pixel telescope in the high multiplicity environment of Pb-Pb collisions. The measurements reported in this paper show that the pixel planes perform extremely well. In the meantime, the complete telescope has been constructed, and was operated in October 2003 with high energy Indium-Indium collisions. Results from that run will be presented in a forthcoming publication.

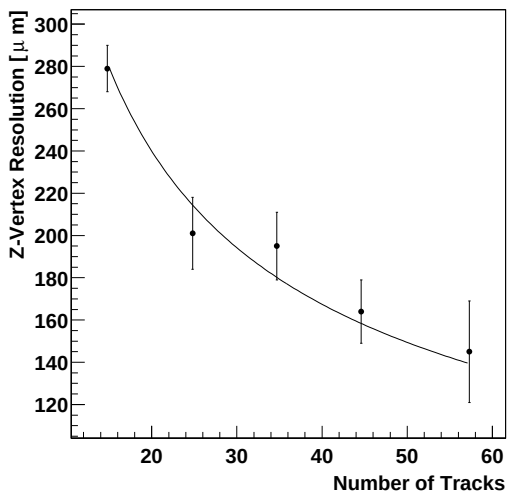

Figure 15: Z-vertex resolution versus the number of tracks associated with the vertex, for the most downstream target.

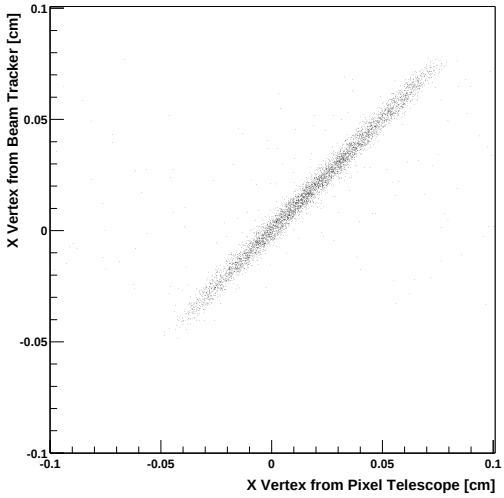

Figure 16: Correlation between the x transverse coordinate of the vertex measured with the beam tracker and the same variable measured by the pixel telescope.

Acknowledgements

We would like to express our gratitude to all the people that helped realising this challenging detector on a short time scale. This detector has been developed within the framework of the NA60 experiment. It is therefore natural to start by thanking our colleagues from NA60. In particular, we express our gratitude to D. Marras for help with the electronics aspects of the project. We very much appreciate the crucial contribution from the EP/ED and EP/MIC groups, and from the ALICE pixel project team, especially M. Campbell, P. Riedler, G. Stefanini and K. Wyllie. We also thank E. David, C. Joram, L. Kottelat, I. McGill and A. Onnela, of the EP/TA1 group, for their invaluable help in the design and construction of the pixel telescope. We are also indebted to R. de Oliveira, C. Millerin and M. Sanchez, of the EST/DEM group, for their contribution to the layout and production of the hybrid circuits.

References

[1] A. Baldit et al., NA60 Proposal, Study of prompt dimuon and charm production with proton and heavy ion beams at the CERN SPS, CERN/SPSC 2000-010, SPSC-P316, March 2000.

[2] K. Wyllie et al., A pixel readout chip for tracking at ALICE and particle identification at LHCb, Proceedings of the Fifth Workshop on Electronics for LHC Experiments, Snowmass, Colorado, 1999.

[3] J.J. van Hunen et al., Irradiation and SPS Beam Tests of the ALICE1LHCb Pixel Chip, CERN-ALI-2001-015, 2001.